

# RXTE monitoring observations of Markarian 3

I. Georgantopoulos<sup>1</sup>, I. Papadakis<sup>2</sup>, R.S. Warwick<sup>3</sup>, D.A. Smith<sup>4,5</sup> G.C. Stewart<sup>3</sup> and R.G. Griffiths<sup>3</sup>

<sup>1</sup> National Observatory of Athens, Lofos Koufou, Palaia Penteli, 15236, Athens, Greece

<sup>2</sup> Physics Department, University of Crete, Heraklion, Greece

<sup>3</sup> Department of Physics and Astronomy, University of Leicester, Leicester, LE1 7RH

<sup>4</sup> Laboratory for High Energy Astrophysics, Code 662, NASA/GSFC, Greenbelt, Maryland, MD20771, USA

<sup>5</sup> Astronomy Department, University of Maryland, College Park, MD 20742, USA

arXiv:astro-ph/9903083v1 5 Mar 1999

19 May 2018

## ABSTRACT

We present Rossi X-ray Timing Explorer, monitoring observations of the Seyfert 2 galaxy Markarian 3 spanning a 200 day period during which time the source flux varied by a factor  $\sim 2$  in the 4–20 keV bandpass. In broad agreement with earlier Ginga results, the average spectrum can be represented in terms of a simple spectral model consisting of a very hard power-law continuum ( $\Gamma \approx 1.1$ ) modified below  $\sim 6$  keV by a high absorbing column ( $N_H \sim 6 \times 10^{23} \text{ cm}^{-2}$ ) together with a high equivalent width Fe-K emission feature at 6.4 keV. The abnormally flat spectral index is probably the signature of a strong reflection component and we consider two models incorporating such emission. In the first the reflected signal suffers the same absorption as the intrinsic continuum, whereas in the second the reflection is treated as an unabsorbed spectral component. In the former case, we require a very strong reflection signal ( $R \lesssim 3$ ) in order to match the data; in addition variability of *both* the intrinsic power-law and the reflection component is required. The unabsorbed reflection model requires a somewhat higher line-of-sight column density to the nuclear source ( $\sim 10^{24} \text{ cm}^{-2}$ ), but in this case the reflected signal remains constant whilst the level of the intrinsic continuum varies. The latter description is consistent with the reflection originating from the illuminated far inner wall of a molecular torus, the nearside of which screens our direct view of the central continuum source.

**Key words:** . galaxies:active – X-ray:galaxies – galaxies:Seyfert – galaxies:individual: Markarian 3

## 1 INTRODUCTION

In recent years the X-ray properties of Seyfert galaxies have been extensively studied (for a review see Mushotzky, Done & Pounds 1993). It was soon realised that Seyfert 2 galaxies exhibit much lower X-ray luminosities, at least in the soft X-ray band below  $\sim 3$  keV, than those typical of Seyfert 1 galaxies, a result which can now be explained in terms of the standard AGN unification model (Antonucci & Miller 1985). According to this paradigm, the nucleus (supermassive black hole, accretion disc and broad line region) has basically the same structure in both types of object but, depending on the circumstances, can be hidden from viewed by a thick molecular torus (Krolik & Begelman 1986). Specifically if the source is observed at a sufficiently high inclination angle, and thus the line of sight intersects the torus, it would be classified as a Seyfert 2, whereas for all other orientations it would be deemed to be a Seyfert 1. As well as obscuring the nucleus in the optical, the molecular torus can strongly suppress soft X-ray emission through the process of photoelectric absorption in cool atomic and molecular gas. In the

limit of very high column densities, Thomson scattering will also diminish the more penetrating hard X-ray emission.

The X-ray spectra of Seyfert 2 galaxies as observed by *Ginga*, *ASCA* and recently *BeppoSAX* have proved to be very complex (e.g. Awaki et al. 1991; Smith & Done 1996; Turner et al. 1997a; Griffiths et al. 1998). In broad terms most Seyfert 2 X-ray spectra can be well fitted by a power-law continuum (typically  $\Gamma \sim 1.8$ ), plus an Fe-K emission line at 6.4 keV and a reflection component (e.g. Lightman & White 1988, George & Fabian 1991). This latter component, which may be produced at the surface of the putative molecular torus, flattens the observed continuum and can dominate the spectrum above  $\sim 10$  keV. In most Seyfert 2s the above emission components are viewed through a large absorbing column density, typically  $N_H > 10^{23} \text{ cm}^{-2}$ . In some sources additional emission in the form of a soft X-ray excess is observed below  $\sim 3$  keV probably as a result of scattering of the intrinsic power-law continuum by a strongly photoionised medium. In order to observe such soft X-ray emission it is clearly a requirement that the scattering

medium should extend, in projection on the sky, well beyond the bounds of the obscuration of the molecular torus.

In contrast to the recent progress in understanding the X-ray spectral characteristics of Seyfert 2 galaxies, our knowledge of their X-ray variability properties remains very limited. According to the standard unification scenario, the hard X-ray continuum should vary with large amplitude in a similar way to that observed in Seyfert 1 galaxies (Mushotzky, Done & Pounds 1993). However, in type 2 objects the accretion disk, if present, is probably viewed at an acute angle and also soft X-rays emanating directly from the nucleus are suppressed. Since the remaining reprocessed spectral components, namely the Fe-K line, the reflection signal and the soft excess, are likely to originate from regions of parsecs scale-size, it follows that significantly less variability might be expected in Seyfert 2 objects, at least in those parts of the spectrum where the reprocessing makes a substantial contribution to the overall flux.

In this paper, we focus on the properties of the Seyfert 2 galaxy Markarian 3 (hereafter Mrk 3) which, at a redshift  $z = 0.0137$ , is one of the brightest and consequently most well-studied, members of its class. *Ginga* observations (Awaki et al. 1990; Awaki et al. 1991; Smith & Done 1996) first revealed an abnormally flat power-law continuum emerging through a high obscuring column ( $N_H \sim 6 \times 10^{23} \text{ cm}^{-2}$ ). A strong Fe line was also detected with a high equivalent width ( $\approx 1.3 \text{ keV}$ ). Mrk 3 has the hardest spectrum of all 16 Seyfert 2 studied by Smith & Done (1996), significantly harder than the spectrum of Seyfert 1 galaxies, thus challenging the standard unification models if the observed continuum actually corresponds to the underlying power-law in this source. However, several other Seyfert 2 galaxies have been found to possess flat spectra and strong Fe lines (e.g. Reynolds et al. 1994; Maiolino et al. 1998; Iwasawa & Comastri 1998) with spectra generally indicating very heavy obscuration along the line of sight and also the presence of a strong Compton reflection component.

Observations of Mrk 3 with the high spectral resolution afforded by the *ASCA* SIS have resolved the Fe-K line into at least two components (Iwasawa et al. 1994). The dominant component at 6.4 keV has an equivalent width of 0.9 keV and a FWHM of  $\sim 10^4 \text{ km s}^{-1}$ , while the second component at 7 keV has an equivalent width of 0.2 keV and appears to be narrower than the first. The same *ASCA* observations (Iwasawa et al. 1994) require a spectral index of  $\Gamma \approx 1.8$  but unfortunately the limited spectral bandpass (0.6–10 keV) of *ASCA* provides only weak constraints on the properties of the intrinsic continuum. A re-analysis of the Mrk 3 spectrum using non-simultaneous *Ginga*, *ROSAT* and *ASCA* observations (Griffiths et al. 1998), covering a wide spectral band (0.1–30 keV), yielded a near canonical value for the power-law,  $\Gamma \approx 1.7$ , when either an additional absorption edge at 8 keV (perhaps originating in a warm absorber), or reflection was included in the spectral model. Recent observations with *BeppoSAX* (Cappi et al. 1999), which extend the spectral coverage to 150 keV, indeed confirm the presence of a steep ( $\Gamma \sim 1.8$ ) intrinsic power-law. Turner et al. (1997) have also re-analysed the *ASCA* data and propose an alternative model in which the intrinsic continuum is viewed through a very large absorbing column ( $N_H > 10^{24} \text{ cm}^{-2}$ ) while the reflection component is unobscured (in contrast to the standard reflection scenario in which the direct power-law and

reflection components are observed through the same  $N_H$ ). The *BeppoSAX* observations (Cappi et al. 1999) again support the above picture. Such a model would be applicable, for example, if we have a direct, unobscured view of the illuminated (far) inner walls of the torus.

Time variability studies can provide additional constraints on the geometry of the nucleus and the surrounding region. Comparison of the *Ginga*, *BBXRT* and the *ASCA* measurements shows a decrease in the 2–10 keV continuum flux by almost a factor of 3 (Iwasawa et al. 1994). During the same period the Fe line flux decreased by a factor of 1.8 (Griffiths et al. 1998), substantially less than the continuum variation. However, Turner et al. (1997) examined the short-term variability using *ASCA* observations but found no significant (<90 per cent) variability on timescales as short as one day.

Here, we present the results of a X-ray monitoring campaign carried out on Mrk 3 by the Rossi X-ray Timing Explorer (*RXTE*) mission, spanning a period of  $\sim 200$  days. Our objective is to use the variability exhibited in the 4–20 keV band to place constraints on the geometry of the Mrk 3 nucleus and any surrounding gaseous media. The extended energy range of the *RXTE* detectors also provides the opportunity to explore further the spectral composition of the X-ray emission emanating from Mrk 3.

## 2 THE OBSERVATIONS

Mrk 3 was observed with the *RXTE* between 25 December 1996 and 6 July 1997. In total 12 observations were obtained, with a duration of about 5 ksec each. We have both Proportional Counter Array (PCA) and High Energy X-ray Timing Experiment (HEXTE) data but here we present the PCA analysis only. The PCA consists of five collimated ( $1^\circ$  FWHM) Xenon proportional counter units (PCU). The PCU are sensitive to energies between 2 and 60 keV. However, the effective area drops very rapidly below 4 and above 20 keV. The energy resolution is 18 per cent at 6.6 keV (Glasser, Odell & Seufert 1994). The collecting area of each PCU is  $1300 \text{ cm}^2$ . We extract PCU light curves and spectra from only the top Xenon layer in order to maximize the signal-to-noise ratio. We use only 3 PCUs (0 to 2); the data from the other two PCU were discarded as these detectors were turned off on some occasions. The data were selected using standard screening criteria: we exclude data taken at an Earth elevation angle of less than  $10^\circ$ , pointing offset less than  $0.01^\circ$  and during and 30 minutes after the satellite passage through the South Atlantic Anomaly (SAA). The resulting total integration time is 59 ksec. In both the spectral and the timing analysis, we use only data between 4 and 20 keV where the effective area is the highest.

We use the PCABACKEST v2 routine of FTOOLS v 4.1.1 to generate the background models which take into account both the cosmic and the internal background. The internal background is estimated by matching the conditions of the observations with those in various model files. Most of the internal background is correlated with the L7 rate, the sum of 7 rates from pairs of adjacent anode wires. However, there is a residual background component correlated with recent passages from the SAA. Therefore, the use of a second, activation component is also necessary. The level

**Table 1.** Log of the 12 RXTE observations

Obs.No.	Date	Count Rate ct s <sup>-1</sup>
1	25/12/96	2.5
2	17/02/97	3.2
3	16/03/97	3.5
4	21/03/97	3.8
5	31/03/97	4.3
6	04/04/97	4.0
7	14/04/97	5.2
8	15/04/97	5.0
9	16/04/97	4.3
10	17/04/97	5.0
11	30/05/97	2.5
12	06/07/97	2.3

of the residual internal background errors after background subtraction with PCABACKEST is about 20 per cent of the cosmic X-ray background  $1\sigma$  fluctuations in the 2-10 keV band. The observation date for each dataset together with the observed background-subtracted count rate in the full 2-60 keV PCA energy band are given in Table 1.

### 3 TIME VARIABILITY

Here, we address the issue of flux and spectral variability in a model independent way, using the background subtracted light curves. We divide the 4 to 20 keV range into 4 bands, namely 4-6 keV and 7-10 keV, where the underlying power-law probably dominates the flux, 6-7 keV where a significant fraction of the flux should originate from the Fe line at 6.4 keV and finally 10-20 keV where the flux is quite possibly dominated by a reflection bump. The light curves for these bands are shown in Fig. 1 with  $\pm 1\sigma$  error bars. It is evident that there is variability in all four bands, with a minimum-to-maximum amplitude of at least a factor of two. This result is statistically significant at a high level of confidence; a constant value for the count rate gives  $\chi^2$  values of 33, 134, 307 and 850 (11 degrees of freedom) for the 4-6, 6-7, 7-10 and 10-20 keV bands respectively. The rms variation in the respective light curves, after correcting for the variance due to the photon statistics, is 15, 17, 22 and 28 per cent. The apparent increase in the fractional variability amplitude towards higher energy might arise, for example, if a less variable or constant spectral component contributes preferentially to the softer bands; however spectral analysis does not substantiate this simple picture (see the next section).

We investigated the possibility of spectral variability by plotting the ratios of the 10-20 keV/7-10 keV and 7-10 keV/4-6 keV count rates, denoted as HR1 and HR2 respectively, as a function of time (see Fig. 1). Both the HR1 and HR2 ratios provide some evidence for such temporal variability; against the constant ratio hypothesis the  $\chi^2$  values are respectively 20 and 27 (for 11 degrees of freedom), corresponding to only a 5 and 0.5 per cent chance probabilities. Hence, the data do suggest the presence of subtle spectral variations, but unfortunately do not provide any strong pointers to a preferred spectral model.

### 4 SPECTRAL ANALYSIS

The PCA data from each observation were binned to give a minimum of 20 counts per channel. All data below 4 and above 20 keV were ignored due to their poor signal-to-noise ratio. By discarding the data below 4 keV we also avoid the complications associated with the soft X-ray excess in this source (e.g. Griffiths et al. 1998). The spectral fitting analysis was carried out using the XSPEC v.10 software package on the basis of “joint simultaneous fits” to the 12 RXTE observations.

Following previous *Ginga* and *ASCA* results, we first employ a very simple spectral model consisting of a power-law continuum, with photon spectral index  $\Gamma$ , modified by absorption in a column density,  $N_H$ , of cool neutral material. A Gaussian line was also included to account for Fe-K emission. For simplicity the line energy and intrinsic width were fixed at the values obtained from *ASCA* by Griffiths et al. (1998), *i.e.*  $E_{line} = 6.38$  keV and  $\sigma_{line} = 0.1$  keV (since consistent values were obtained in free fits of these parameters). The values of the  $N_H$ , the photon index and the normalization of the Fe line are free parameters but they are tied to the same value. However, the normalizations of the power law are allowed to vary freely. The results of fitting this spectral model are presented in Table 2 as model A, where the errors correspond to the 90 per cent confidence level for one interesting parameter. The derived photon index is very flat ( $\Gamma \approx 1.1$ ), consistent with the original Smith & Done (1996) analysis of the *Ginga* data. The resulting  $\chi^2$  of 365 for 489 degrees of freedom (dof) implies an excellent fit (although the errors arising from the background model, may have been somewhat overestimated). Fig. 2 shows a typical PCA count rate spectrum from a single observation, together with the best-fitting model prediction and the resulting residuals. As can be seen from Fig. 2 we clearly observe signal up to 20 keV, even in the case of the lowest flux observations.

The derived Fe-K line flux was  $4.7 \pm 0.84 \times 10^{-5}$  photon s<sup>-1</sup> cm<sup>-2</sup> implying an equivalent width varying from 1.4 keV (observation 12) to 0.4 keV (observation 2). The flux of the Fe line is entirely consistent with that obtained by Iwasawa et al. (1994). When the normalisation of the Fe-K component was “untied” across the set of observations, the resulting  $\chi^2$  reduced to 357 for 478 dof, but this is not a statistically significant improvement (according to the F-test for 11 additional parameters). We conclude that there is no strong evidence for variability in the Fe-K line flux in the RXTE data. In fact this conclusion holds for all spectral models (models A-D) considered in this section, and so in each case we have kept the Fe-K normalisation tied to a single value for all the datasets.

The next step was to investigate whether there is any evidence for changes in either the photon spectral index or the column density. The result of spectral fitting with each of these parameters in turn “untied” was a  $\chi^2$  of 337 and 335 respectively for 478 dof. In both cases the change in  $\chi^2$  (compared to model A) is statistically significant at over 99 per cent confidence. The range of the apparent variation in the spectral index is  $\Gamma = 0.94^{+0.16}_{-0.16}$  to  $1.54^{+0.35}_{-0.29}$  while the best fit column density is  $N_H = 66^{+5}_{-9} \times 10^{22}$  cm<sup>-2</sup>. Similarly, when the  $N_H$  is untied we obtain  $N_H = 47^{+6}_{-6}$  to  $69^{+5}_{-5} \times 10^{22}$  cm<sup>-2</sup> while the best fit photon index is  $\Gamma = 1.14^{+0.11}_{-0.11}$ . This confirms the evidence from the hardness ratios for underlying

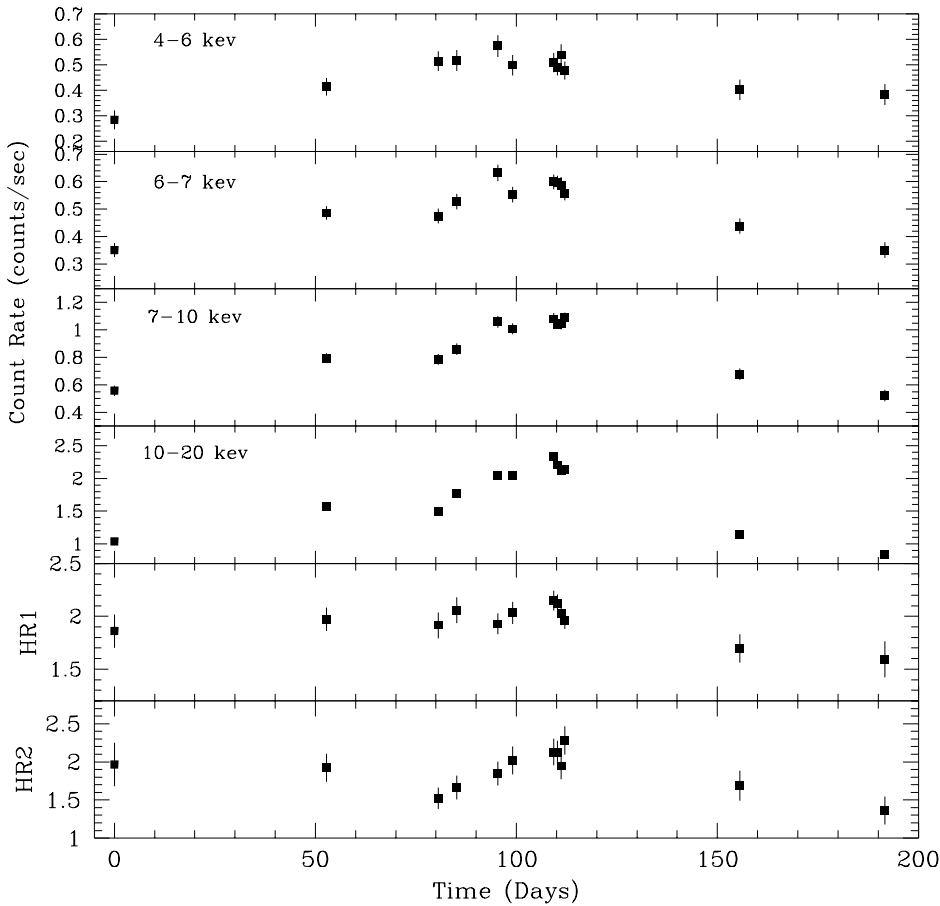


**Figure 1.** The background subtracted light curves in four different energy bands (upper panels). Plots of the 10–20 keV/7–10 keV (HR1) and 7–10 keV/4–6 keV (HR2) hardness ratios as a function of time are also shown (lower two panels).

**Table 2.** Results from the spectral fitting of the 12 *RXTE* datasets

Model	$N_H$	$\Gamma$	R	$E_{edge}$	$\tau$	$\chi^2/\text{dof}$
A	$63_{-4}^{+4}$	$1.06_{-0.06}^{+0.04}$	-	-	-	365/489
B	$75_{-3}^{+3}$	1.8	$0.1_{-0.1}^{+1.0} - 3.4_{-0.5}^{+0.5}$	-	-	337/478
C	$110_{-6}^{+6}$	$1.85_{-0.09}^{+0.09}$	$0.7_{-0.14}^{+0.14} - 2.5_{-0.5}^{+0.5}$	-	-	322/489
D	$74_{-3}^{+3}$	$1.3_{-0.14}^{+0.14}$	-	8.1	0.24	376/489

spectral variability. Note that there is clearly a dependence of the photon index on the column density in the sense that the data cannot easily discriminate between a flat photon index and a high column density.

As an additional test, we checked for possible spectral variations correlated with the X-ray brightness of the source. For this purpose we separated the observations into high and low-states on the basis a flux threshold of  $3 \times 10^{-11}$  erg cm $^{-2}$  s $^{-1}$  in the 4–20 keV band. Observations 4–10 were thereby classified as high state, with observations 1–3 and 11–12 comprising the low-state. The results (based on the model A prescription) are summarised in Fig. 3 where we plot the joint 68, 90 and 99 per cent confidence contours in the  $\Gamma$  versus  $N_H$  plane for the high-flux and the low-

flux states. We see that although the best fit centroids are offset, the 90 per cent confidence contours show considerable overlap, suggesting that we cannot be confident that either the continuum slope or column density shows any consistent change with increasing flux.

Although, the model A prescription defined above gives an acceptable fit in terms of the  $\chi^2$  statistic, there is evidence from both *ASCA* and *Ginga* observations (Griffiths et al. 1998) and recently *BeppoSAX* observations (Cappi et al. 1999) that the anomalously flat power-slope derived for Mrk 3 is due to the presence of Compton reflection. The next step in the current analysis was therefore to include a reflection component in the spectral modelling. Specifically we use the PEXRAV model (Magdziarz & Zdziarski 1995) in XSPEC.

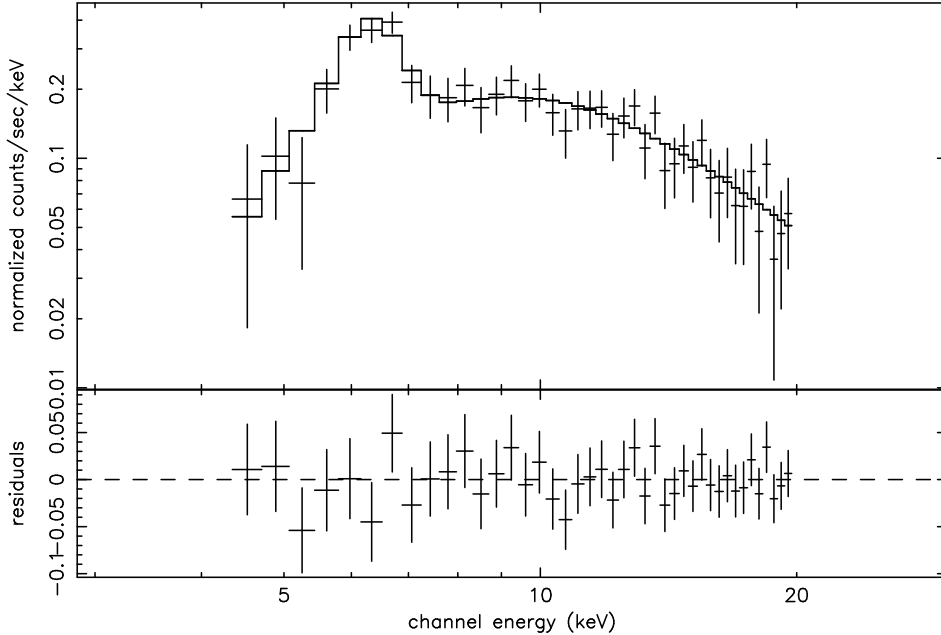


**Figure 2.** The RXTE PCA spectrum of Mrk 3 from observation 1. The solid line corresponds to the best fitting version of model A after folding through the instrument response. The lower panel shows the corresponding residuals to the fit.

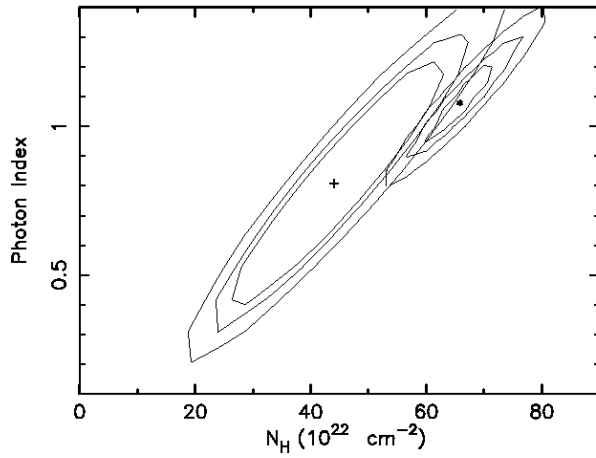


**Figure 3.** The  $\Gamma - N_H$  contours for the high-flux (rightmost) and the low-flux data (leftmost); in each case the three levels correspond to 68, 90 and 99 per cent confidence contours.

We initially assume that both the reflection component and the power-law are absorbed by the cold gas column density according to the standard reflection prescription. The strength of the reflection component is governed by the parameter  $R$ , representing the strength of the reflected signal relative to the level of the incident power-law continuum. Following the results of Griffiths et al. (1998), we fix the inclination angle for the disk at  $i = 60^\circ$ ; this large inclination angle implies that a large part of the reflection component originates in the torus. We also set the spectral index of the power-law continuum to ( $\Gamma = 1.8$ ) following the results of

Griffiths et al. (1998) and Cappi et al. (1999). Note that without this constraint the fit reverts to a very flat power-law slope and negligible reflection. Our initial approach was to tie the *effective normalisation* of the reflection signal to a single value across the set of observations. The resulting best-fitting model gave a  $\chi^2$  of 395 for 489 dof and required values of  $R$  varying from  $0.7 \pm 0.2$ – $2.1 \pm 0.9$ . In this model even though the reflection component has a fixed level,  $R$  changes since the normalisation of the intrinsic power-law varies from observation to observation. However, when we allow the normalisation of the reflection component to vary freely, we obtain a  $\Delta\chi^2 \approx 58$  which is highly statistically significant. Details of this fit are summarised in Table 2 (Model B) and Fig. 4 shows the derived temporal variation in the normalisation of both the power-law and reflection components. There is clearly a suggestion that the latter responds to variations in the former with any lag between the two being  $\lesssim 1$  month. Unfortunately there is insufficient data to set a more precise constraint.

As noted earlier an alternative reflection model for Mrk 3 was proposed by Turner et al. (1997) in which the intrinsic power-law is seen through an increased column but the reflection is largely unobscured. The application of such a model to the RXTE data gives the results presented in Table 2 (model C) when the reflection normalisations are tied to a single value. The best-fitting power-law slope is  $\Gamma = 1.85^{+0.09}_{-0.09}$ , consistent with the canonical AGN power-law, and  $N_H = 1.1 \times 10^{24} \text{ cm}^{-2}$ , *i.e.* approximately 30% higher than the value obtained earlier (as model B). Note that at such high column densities the effects of Thomson scattering become important. Then the derived column density from fitting simple absorption models will overestimate the true column (Leahy et al. 1989). The model above gives the lowest reduced  $\chi^2$  of all the models we consider ( $\chi^2 = 322/489$ ). Comparison with the standard reflection model (in the case where the reflection component has a

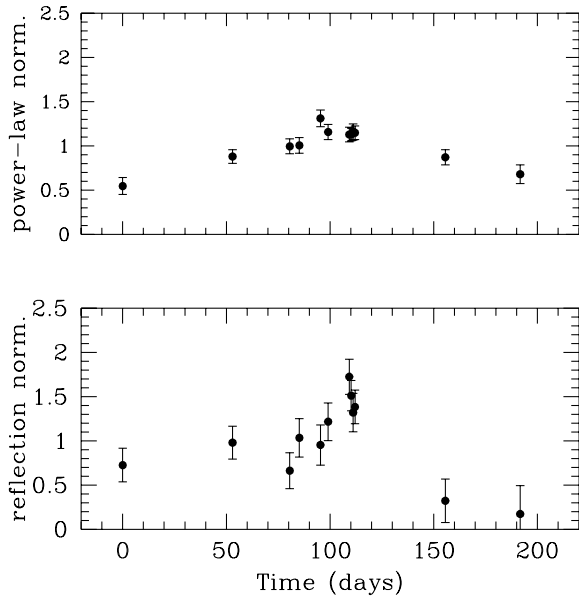


**Figure 4.** The normalization of the power-law (top) and the reflection components (bottom) in the case of the standard reflection model (model B). The errors correspond to a 90 per cent confidence level.

constant normalisation) using the F-test, suggests that the Turner et al. model represents a better fit to the data at the 90 per cent confidence level. Interestingly in this second reflection scenario we obtain only a small improvement in the  $\chi^2$  ( $\Delta\chi^2 \sim 6$ ) when the normalisation of the reflection component is allowed to vary across the observations. Thus in this description the reflection component essentially remains constant.

Finally, we note that Griffiths et al. (1998) suggest an alternative explanation for the abnormally flat spectrum of Mrk 3. These authors include an additional absorption edge near 8 keV in their spectral model which serves to steepen the slope determined for the underlying power-law component. The edge feature could originate in a putative warm absorber (e.g. Reynolds 1997; George et al. 1998) which in the case of Mrk 3 may also produce the scattered soft excess flux observed below 3 keV (assuming an extensive distribution of this hot medium in the nuclear region of the galaxy). We have therefore also considered the effect of including such a feature in the spectral fitting of the *RXTE* datasets. The results are given in Table 2 (model D), where we have fixed the edge energy and optical depth at the values obtained by Griffiths et al. (*i.e.*  $E_{\text{edge}} = 8.1$  keV,  $\tau = 0.24$ ). In this case the power-law remains flat ( $\Gamma \approx 1.3$ ) and the best fit is actually worse than that obtained in the absorbed power-law model (model A). We conclude that the absorption edge alone is not sufficient to explain the apparently anomalously hard spectrum measured for Mrk 3 by *RXTE*.

## 5 DISCUSSION

The *RXTE* observations presented in this paper confirm the finding of previous studies namely that the X-ray continuum emanating from Mrk 3 is exceptionally hard, at least within the 4-20 keV bandpass. The preferred interpretation of this

flat spectrum is that this source exhibits particularly strong Compton reflection and we find that two variants on this reflection theme are broadly consistent with the *RXTE* data both in terms of the average spectrum and the observation to observation spectral variability.

In the standard reflection description (e.g. Griffiths et al. 1998) the intrinsic power-law continuum, the reflection component and the Fe-K emission are all affected by photoelectric absorption in a large column density of cool absorbing gas (with  $N_H \sim 7 \times 10^{23} \text{ cm}^{-2}$ ). In this model both the continuum and the reflected component vary together; with any lag in the response of the latter constrained to  $\lesssim 1$  month. In contrast, the *RXTE* data show no evidence for variability in the Fe line flux. It is quite plausible that the (bulk of the) Fe-K flux and the reflection signal originate in different regions. For example a significant fraction of the Fe-K line flux might originate in a very extended region which is optically thin to Fe-K photons whereas the reflection could arise in a partially covering screen of optically thick clouds situated within a light month of the nucleus.

In the alternative version of the reflection model (e.g. Turner et al. 1998) our line of sight to the reflecting material is largely unobscured, although the nucleus itself is covered by a very substantial screen of absorption ( $N_H \sim 10^{24} \text{ cm}^{-2}$ ). This model actually gave the best fit to the average spectrum and a fairly canonical value for the intrinsic power-law slope. Also the only temporal variation required is in the level of the underlying continuum. This leads to arguably the most plausible explanation of the anomalously hard spectrum observed in Mrk 3, namely that we see strong Compton reflection from the far illuminated wall of a putative molecular torus in its nucleus. Presumably our line of sight to this region passes over the nearside of the torus without intercepting anything like the column density that lies directly in front of the central nuclear source.

Future monitoring observations by satellites such as XMM will greatly improve the photon statistics as well as the spectral resolution and thus are expected to shed further light on the detailed geometry of the central region of Mrk 3. Such observations will in fact provide a critical and detailed test of current unification schemes.

## 6 ACKNOWLEDGEMENTS

We thank the anonymous referee for many useful comments and suggestions. RGG acknowledges support from PPARC in the form of a research studentship.

## REFERENCES

- Antonucci, R.R.J., Miller, J.S., 1985, ApJ, 297, 621
- Awaki, H., Koyama, K., Kunieda H., Tawara, Y., 1990, Nature, 346, 544
- Awaki, H., Koyama, K., Inoue, H., Halpern, J.P., 1991, PASJ, 43, 195
- Cappi, M., et al., 1999, A&A, in press
- George, I.M., Fabian, A.C., 1991, MNRAS, 249, 352
- George, I.M., Turner, T.J., Netzer, N., Mandra, K., Mushotzky, R.F., Yaqoob, T., 1998, ApJS, 114, 73
- Glasser, C.A., Odell, C.E., Seufert, S.E., 1994, IEEE Trans.

Nucl. Sci., 41, 4

Griffiths, R.E., Warwick, R.S., Georgantopoulos, I., Done, C., Smith, D.A., 1998, MNRAS, 298, 1159

Iwasawa, K., Yaqoob, T., Awaki, H., Ogasaka, Y., 1994, PASJ, 46, L167

Iwasawa, K., Comastri, A., 1998, MNRAS, 297, 1219

Krolik, J.H., Begelman, M.C., 1986, ApJ, 308, 55

Lee, J.C., Fabian, A.C., Reynolds, C.S., Iwasawa, K., Brandt, W.N., 1998, MNRAS, 300, 583

Leahy, D.A., Matsuoka, M., Kawai, N., Makino, F., 1989, MNRAS, 236, 603

Lightman, A.P., White, T.R., 1988, ApJ, 335, 57

Maiolino, R., Salvati, M., Bassani, L., Dadina, M., Della Ceca, R., Matt, G., Risaliti, G., Zamorani, G., 1998, A&A, 338, 781

Magdziarz, P., Zdziarski, A., 1995, MNRAS, 273, 837

Mushotzky, R.F., Done, R.F., Pounds, K.A., 1993, ARA&A, 31, 717

Smith, D.A., Done, C., 1996, MNRAS, 280, 355

Nandra, K., Pounds, K.A., 1994, MNRAS, 268, 405

Nandra, K., Mushotzky, R.F., Yaqoob, T., George, I.M., Turner, T.J., 1997, MNRAS, 284, L10

Reynolds, C.S., 1997, MNRAS, 286, 513

Reynolds, C.S., Fabian, A.C., Makishima, K., Fukazawa, Y., Tamura, T., 1994, MNRAS, 268, L55

Turner, T.J., George, I.M., Nandra, K., Mushotzky, R.F., 1997, ApJS, 113, 23

Turner, T.J., George, I.M., Nandra, K., Mushotzky, R.F., 1997, ApJ, 488, 164